

Emergent quasi-one-dimensionality in a kagomé magnet: A simple route to complexity

Shou-Shu Gong¹, Wei Zhu², Kun Yang³, Oleg A. Starykh⁴, D. N. Sheng², and Leon Balents⁵

¹*National High Magnetic Field Laboratory, Florida State University, Tallahassee, FL 32310*

²*Department of Physics and Astronomy, California State University, Northridge, CA 91330*

³*National High Magnetic Field Laboratory and Department of Physics, Florida State University, Tallahassee, FL 32306*

⁴*Department of Physics and Astronomy, University of Utah, Salt Lake City, UT 84112*

⁵*Kavli Institute for Theoretical Physics, University of California, Santa Barbara, CA 93106*

We study the ground state phase diagram of the quantum spin-1/2 Heisenberg model on the kagomé lattice with first- ($J_1 < 0$), second- ($J_2 < 0$), and third-neighbor interactions ($J_d > 0$) by means of analytical low-energy field theory and numerical density-matrix renormalization group (DMRG) studies. The results offer a consistent picture of the J_d -dominant regime in terms of three sets of spin chains weakly coupled by the ferromagnetic inter-chain interactions $J_{1,2}$. When either J_1 or J_2 is much stronger than the other one, the model is found to support one of two cuboctohedral phases, cuboc1 and cuboc2. These cuboc states host non-coplanar long-ranged magnetic order and possess finite scalar spin chirality. However, in the compensated regime $J_1 \simeq J_2$, a valence bond crystal phase emerges between the two cuboc phases. We find excellent agreement between an analytical theory based on coupled spin chains and unbiased DMRG calculations, including at a very detailed level of comparison of the structure of the valence bond crystal state. To our knowledge, this is the first such comprehensive understanding of a highly frustrated two-dimensional quantum antiferromagnet. We find no evidence of either the one-dimensional gapless spin liquid or the chiral spin liquids, which were previously suggested by parton mean field theories.

PACS numbers: 73.43.Nq, 75.10.Jm, 75.10.Kt

I. INTRODUCTION

The kagomé lattice, from its humble origin in the hands of fishermen, now sits at the forefront of the search for exotic quantum phases of matter such as quantum spin liquids [1, 2]. Compelling numerical evidence shows that, on this lattice, even the simplest model of magnetism, the Heisenberg spin-1/2 Hamiltonian with up to third neighbor interactions, shows not just one but at least two of these highly entangled phases [3–28]. The vast majority of studies have naturally focused on the regime in which antiferromagnetic nearest-neighbor coupling is dominant. Recently, however, theory and experiment have turned to a different limit, of dominant antiferromagnetic *third-neighbor* interaction J_d (of a particular type, across the diagonal of the kagomé lattice), in the material kapellasite, $\text{Cu}_3\text{Zn}(\text{OH})_6\text{Cl}_2$ [29–34]. In this regime, the proposed model, which also has the ferromagnetic J_1, J_2 couplings, classically supports interesting non-coplanar ground states with spins pointing to the corners of a cuboctahedron, a state which leaves no residual continuous subgroup of $\text{SU}(2)$ spin-rotation symmetry unbroken, and possesses spontaneous non-zero scalar spin chirality [35]. It has been suggested based on mean-field and variational parton constructions that for $S = 1/2$ quantum fluctuations may overcome these orders, leading to chiral quantum spin liquid ground states [36].

In the large- J_d limit, the kagomé lattice separates into a mesh-like set of three kinds of one-dimensional (1d) chains oriented at $\pm 120^\circ$ to each other. We show that such a separation is more than just a geometric curiosity. It allows us to capture *all* the low-energy degrees of freedom of the model, including those of the emergent non-local dimer fluctuations. A careful analysis of the residual inter-chain interactions, all of which are represented by the weak J_1 and J_2

bonds, offers us a complete understanding of the phases of this strongly frustrated two-dimensional (2d) spin-1/2 Heisenberg model. We find the phase diagram to contain two cuboctohedral phases, denoted cuboc1 and cuboc2, separated by a region of valence bond crystal (VBC) order. Deep in the analytical limit with $|J_1|, |J_2| \ll J_d$, but J_1/J_2 arbitrary, we obtain asymptotically exact results for the phase boundaries between these three phases. Our analytical approach is nicely complemented by highly accurate numerical Density Matrix Renormalization Group (DMRG) computations on kagomé cylinders of two different geometries, with a circumference of up to 12 sites. Our numerical results strongly support the phase diagram consisting of two cuboc and VBC phases as predicted analytically. We find *no* evidence of the suggested chiral spin liquid states, either analytically or numerically, which puts the validity of the parton approximation for this problem [36] into question. At small J_1, J_2 , this agrees with a pseudofermion functional renormalization group calculation [37], which however finds a spin liquid state for intermediate J_1 , which we do not observe. Profound implications of our findings, both for the minimal theoretical model of kapellasite and for the physics of the real material, are discussed in the concluding section of the paper.

II. ANALYTICAL TREATMENT

A. Mapping to coupled chains and scaling operators

We consider the Heisenberg Hamiltonian,

$$H = J_1 \sum_{\langle i,j \rangle} \mathbf{S}_i \cdot \mathbf{S}_j + J_2 \sum_{\langle\langle i,j \rangle\rangle} \mathbf{S}_i \cdot \mathbf{S}_j + J_d \sum_{\langle\langle\langle i,j \rangle\rangle\rangle_d} \mathbf{S}_i \cdot \mathbf{S}_j, \quad (1)$$

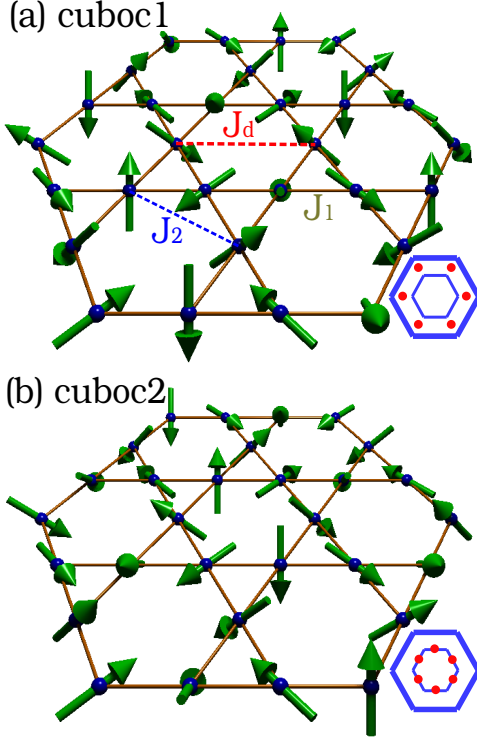


FIG. 1: (Color online) Spin configuration in the ordered cuboc states on kagomé lattice. The arrows indicate the direction of static moments. (a) Cuboc1 state. In this state, the spins on triangles are coplanar. In each hexagon, sets of three consecutive spins are non-coplanar. The J_1, J_2, J_d bonds denote the Heisenberg interactions of the Hamiltonian Eq. (1). (b) Cuboc2 state. In this state, the spins on triangles are non-coplanar and those on hexagons are coplanar. The insets indicate the static spin structure factors for the cuboc states in momentum space with the peaks shown by red dots. The smaller hexagon is the Brillouin zone of the kagomé lattice, and the larger one is the extended Brillouin zone of the extended triangular lattice by adding a virtual site in the center of each hexagon on kagomé lattice.

where the respective interactions are as shown in Fig. 1(a). To make analytic progress, we assume $|J_1|, |J_2| \ll J_d$. Then the exchanges J_1, J_2 have substantial effects only at low energy, and we can use the field theory representation in this regime for the disjoint one dimensional chains generated by J_d alone. These chains form three families, oriented at 120° to one another. Within each family, we take x the coordinate along the chain and y to label the chain itself, with x, y integers. Taking the nearest-neighbor lattice spacing to unity, we define primitive lattice vectors $\mathbf{a}_1 = (2, 0)$, $\mathbf{a}_2 = (-1, \sqrt{3})$, and $\mathbf{a}_3 = -\mathbf{a}_1 - \mathbf{a}_2$, which connect unit cells. The spin on chain of type $q = 1, 2, 3$ with “chain” coordinates x, y is located in real space at $\mathbf{x} = (x + \frac{1}{2})\mathbf{a}_q + y\mathbf{a}_{q+1}$, where here and in the following we treat q as periodic, i.e. $q = 3 + 1 \equiv 1$. For an isotropic system, the total number of sites is $\mathcal{N} = 3L^2$, where L is both the number of sites in a chain (range of x) and the number of chains of a single orientation (range of y). In this chain notation, we can rewrite the interchain in-

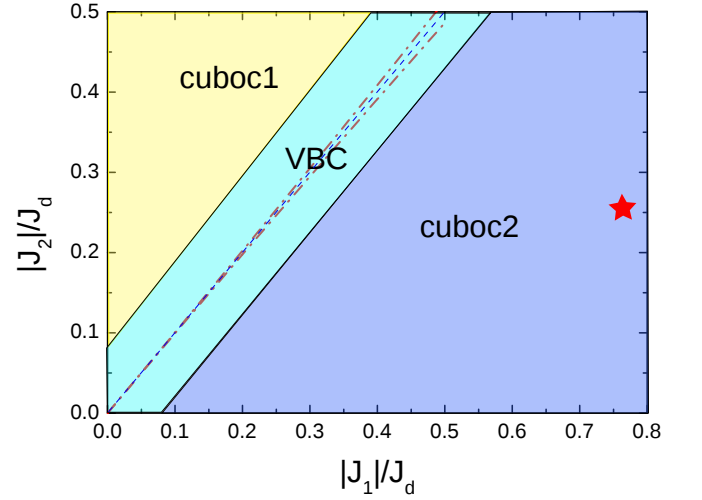


FIG. 2: (Color online) Quantum phase diagram of the spin-1/2 J_1 - J_2 - J_d kagomé model. The short-dashed (blue) lines denote the classical phase boundary separating the cuboc1 and cuboc2 phases [36]. For the spin-1/2 Hamiltonian Eq. (1), the direct phase transition between the two cuboc phases is replaced by the 24-fold degenerate spontaneously dimerized VBC phase (see Sec. II B 2 for the analysis). The two-dimensional phase boundaries with the cuboc states are shown by the dot-dashed (red) lines (see Eq. (28)), which form the wedge-like shape of the 2d VBC phase. The DMRG calculations on open cylinders with different geometries (see Sec. III) find a wider dimerized region, as indicated by the cyan-colored stripe centered around the compensated line $J_1 = J_2$. The symmetries of the dimer order found in DMRG are fully consistent with those of the two-dimensional VBC phase. The enhancement of the VBC order in the cylinder geometry is caused by the strong finite size effects due to open boundary conditions. The red star represents parameters best describing kapellasite [38].

teractions as

$$\begin{aligned}
 H' = & J_1 \sum_{y,y'} \sum_q (\mathbf{S}_{q,y}(-y') \cdot \mathbf{S}_{q+1,y'}(y+y'-1) \\
 & + \mathbf{S}_{q,y}(-y'-1) \cdot \mathbf{S}_{q+1,y'}(y+y')) \\
 & + J_2 \sum_{y,y'} \sum_q (\mathbf{S}_{q,y}(-y'-1) \cdot \mathbf{S}_{q+1,y'}(y+y'-1) \\
 & + \mathbf{S}_{q,y}(-y') \cdot \mathbf{S}_{q+1,y'}(y+y')), \quad (2)
 \end{aligned}$$

where $\mathbf{S}_{q,y}(x)$ is the spin in chain coordinates.

At low energy, each chain, labeled by q and y , is described by a Wess-Zumino-Witten (WZW) $SU(2)_1$ theory, which has primary fields $N_{q,y}$ and $\varepsilon_{q,y}$, describing staggered magnetization (Néel) and staggered dimerization, respectively, as well as chiral $SU(2)$ currents $\mathbf{J}_{q,y,R}, \mathbf{J}_{q,y,L}$. The lattice spin operators decompose into

$$\mathbf{S}_{q,y}(x) = (-1)^x \mathbf{N}_{q,y}(x) + \mathbf{M}_{q,y}(x), \quad (3)$$

where $\mathbf{M} = \mathbf{J}_R + \mathbf{J}_L$ is the uniform magnetization. The fields $\mathbf{N}_{q,y}(x)$ and $\mathbf{M}_{q,y}(x)$ can be treated as slowly-varying functions of x . The primary fields have scaling dimension $\Delta = 1/2$, and represent the strongest correlations of Heisenberg chains. The currents have larger scaling dimension $\Delta = 1$,

and so are less important within interactions than the primary fields. Hence the dominant interaction is generically given by using Eq. (3) and keeping the Néel fields alone:

$$H'_{\text{dom}} \sim 2(J_2 - J_1) \sum_q \sum_{y,y'} (-1)^y \mathbf{N}_{q,y}(-y') \cdot \mathbf{N}_{q+1,y'}(y+y'). \quad (4)$$

We observe that J_1 and J_2 give identical contributions in this

leading approximation, only of opposite sign. This leads to a vanishing along the compensated line $J_1 = J_2$. In the vicinity of this line, otherwise sub-dominant terms will play a role. At the lattice level, the compensation is already evident, as we can rewrite Eq. (2) in this case as

$$H'|_{J_1=J_2} = J_1 \sum_{y,y'} \sum_q (\mathbf{S}_{q,y}(-y') + \mathbf{S}_{q,y}(-y' - 1)) \cdot (\mathbf{S}_{q+1,y'}(y+y') + \mathbf{S}_{q+1,y'}(y+y' - 1)). \quad (5)$$

This symmetric form can be seen directly from examination of the interactions between two chains that cross at a given hexagon, see Fig. 3. Now using Eq. (3), the leading scaling term becomes

$$H'_{\text{sub-dom}}|_{J_1=J_2} \sim J_1 \sum_{y,y'} \sum_q \left(2\mathbf{M}_{q,y}(-y') + (-1)^{y'} \partial_x \mathbf{N}_{q,y}(-y') \right) \cdot \left(2\mathbf{M}_{q+1,y'}(y+y') + (-1)^{y+y'} \partial_x \mathbf{N}_{q+1,y'}(y+y') \right) \quad (6)$$

The term in Eq. (6) is only important when the leading one in Eq. (4) is nearly zero, so it is legitimate to take $J_1 \approx J_2$ in the former.

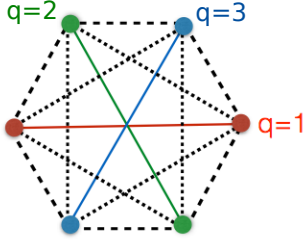


FIG. 3: (Color online) An elementary hexagon of the kagomé lattice. The three types of chains formed by J_d couplings, labeled $q = 1, 2, 3$, are shown in different colors. Interchain interactions J_1 (J_2) are shown by dashed (dotted) lines. Observe that for $J_1 = J_2$ the interchain interaction can be written as a scalar product of sums of pairs of spins from chains with different q 's, as written in Eq. (5). The total interchain Hamiltonian is given by the sum over all hexagons of the lattice.

B. Two dimensional analysis

The leading interactions in Eq. (4) and the sub-dominant corrections in Eq. (6) can be analyzed directly for the two-dimensional infinite system, following methods developed for other coupled chain systems. The closest analogy is that for the planar pyrochlore lattice in Ref. 39.

1. Magnetically ordered region

Away from the compensated line, it is sufficient to consider the dominant term in Eq. (4). At a naïve scaling level, since this interaction is represented in field theory by a term in the effective actions $S' = \int d\tau H'$, and each \mathbf{N} field has dimension $\Delta[\mathbf{N}] = 1/2$, the interaction is marginal. However, as shown in Ref. 39, the presence of a number of such terms proportional to the system volume amplifies its effect, inducing magnetic order with a strength that is power-law in the coupling $(J_1 - J_2)$. This can be verified by using chain mean field theory, in which each chain is treated exactly but the interaction between chains is decoupled in mean field fashion. It can be formulated as a variational approximation, with the variational state the ground state of a fiduciary mean field Hamiltonian, which is

$$H_{\text{MF}} = H_0 - \sum_{q,y} \int d\mathbf{x} \mathbf{h}_{q,y} \cdot \mathbf{N}_{q,y}(\mathbf{x}), \quad (7)$$

where $H_0 = H|_{J_1=J_2=0}$ and $\mathbf{h}_{q,y}$ are effective staggered fields for each chain, which are treated as variational parameters. The variational energy is

$$E_{\text{var}} = \langle H_0 \rangle - E_0 + \langle H'_{\text{dom}} \rangle, \quad (8)$$

where the expectation values are taken in the variational state, and for convenience we subtracted the energy E_0 of pure Heisenberg chains so that the zero of energy is realized at $J_1 = J_2 = 0$. This can be simplified using the fact that $\tilde{\mathbf{N}}_{q,y} \equiv \langle \mathbf{N}_{q,y}(\mathbf{x}) \rangle = \alpha |\mathbf{h}_{q,y}|^{1/3} \hat{\mathbf{h}}_{q,y}$, where α is a constant, which follows from the spin-rotation symmetry of H_0 and the scaling dimension of \mathbf{N} [40]. Similarly, the mean-field energy obeys $\langle H_{\text{MF}} \rangle = E_0 - \frac{3}{4} \alpha \mathcal{L} \sum_{q,y} |\mathbf{h}_{q,y}|^{4/3}$. We can therefore express all variational energies in terms of $\tilde{\mathbf{N}}_{q,y}$, using

Eq. (7) to obtain

$$E_{\text{var}} = \frac{L}{4\alpha^3} \sum_{q,y} |\tilde{N}_{q,y}|^4 - \lambda \sum_q \sum_{y,y'} (-1)^y \tilde{N}_{q,y} \cdot \tilde{N}_{q+1,y'}, \quad (9)$$

where $\lambda = 2(J_1 - J_2)$. The instability to ordering is evident from the fact that interaction (second) term, which can be made negative by a suitable variational choice, is quadratic in \tilde{N} , and hence dominates over the first term, which is quartic, for small \tilde{N} . This implies that E_{var} always has a non-trivial global minimum, even for arbitrarily small λ . The task is now to find this minimum.

To do so, we assume that $|\tilde{N}_{q,y}| = \tilde{N}$ is constant for all chains. Then we minimize the second term over the orientations $\hat{N}_{q,y} = \tilde{N}_{q,y}/|\tilde{N}_{q,y}|$, and after this finally minimize over \tilde{N} . We can rewrite the variational energy as

$$\frac{E_{\text{var}}}{\mathcal{N}} = \frac{1}{4\alpha^3} \tilde{N}^4 - \frac{\lambda}{3} \tilde{N}^2 \sum_q \mathbf{V}_q \cdot \mathbf{W}_{q+1}, \quad (10)$$

where

$$\mathbf{V}_q = \frac{1}{L} \sum_y (-1)^y \hat{N}_{q,y}, \quad \mathbf{W}_q = \frac{1}{L} \sum_y \hat{N}_{q,y}. \quad (11)$$

and the fixed magnitude constraint implies that

$$|\mathbf{V}_q| = |\mathbf{W}_q| = 1, \quad \mathbf{V}_q \cdot \mathbf{W}_q = 0. \quad (12)$$

Obviously the λ term is bounded below by $-|\lambda|\tilde{N}^2$, which is achieved if and only if $\mathbf{V}_q \cdot \mathbf{W}_{q+1} = \text{sign}(\lambda)$. The general solution of these conditions is

$$\mathbf{V}_q = \hat{\mathbf{e}}_{q+1}, \quad \mathbf{W}_q = \text{sign}(\lambda) \hat{\mathbf{e}}_q, \quad (13)$$

where $\hat{\mathbf{e}}_1, \hat{\mathbf{e}}_2, \hat{\mathbf{e}}_3$ are three orthonormal vectors. Finally minimization gives

$$\tilde{N} = \sqrt{2\alpha^3|\lambda|} \quad (14)$$

and $E_{\text{var}} = -\alpha^3 \lambda^2 \mathcal{N}$. We see that the ordered moment grows as the square root of the inter-chain couplings, when we are away from the compensated line.

Clearly the solutions in Eq. (13) represent non-coplanar magnetically ordered configurations. In fact these are exactly the cuboc1 ($\lambda > 0$) and cuboc2 ($\lambda < 0$) states expected classically. On chains of type q , the ordered moments are oriented along the four directions $\hat{\mathbf{e}}_q + \hat{\mathbf{e}}_{q+1}, -\hat{\mathbf{e}}_q - \hat{\mathbf{e}}_{q+1}, \hat{\mathbf{e}}_q - \hat{\mathbf{e}}_{q+1}, -\hat{\mathbf{e}}_q + \hat{\mathbf{e}}_{q+1}$, and all spins together define 12 unique sublattices. Spins along any given chain are all collinear, and alternate in a normal Néel pattern. The state also has non-zero scalar chirality, which is of order \tilde{N}^3 and hence parametrically smaller than the ordered moment in the weakly coupled chain limit. The sign of the scalar chirality is a discrete order parameter and proportional to the triple product $\hat{\mathbf{e}}_1 \cdot (\hat{\mathbf{e}}_2 \times \hat{\mathbf{e}}_3)$.

To see this, it is convenient to write $\mathbf{V}_q = (\hat{N}_q^{(e)} - \hat{N}_q^{(o)})/2$ and $\mathbf{W}_q = (\hat{N}_q^{(e)} + \hat{N}_q^{(o)})/2$ in terms of unit fields on *even*, $\hat{N}_q^{(e)} = \hat{N}_{q,y=\text{even}}$, and *odd*, $\hat{N}_q^{(o)} = \hat{N}_{q,y=\text{odd}}$, chains of type q .

Then Eq. (13) tells that $\hat{N}_q^{(e/o)} = \text{sign}(\lambda) \hat{\mathbf{e}}_q \pm \hat{\mathbf{e}}_{q+1}$. Therefore, using Eqs. (3) and (14), our chain mean-field theory predicts for the expectation value of the lattice spin

$$\mathbf{S}_{q,y}(\mathbf{x}) = \sqrt{2\alpha^3|\lambda|} (-1)^x (\text{sign}(\lambda) \hat{\mathbf{e}}_q + (-1)^y \hat{\mathbf{e}}_{q+1}). \quad (15)$$

This means that the two-point spin correlations reduce to

$$\begin{aligned} \mathbf{S}_{q,y}(\mathbf{x}) \cdot \mathbf{S}_{q',y'}(\mathbf{x}') &= 2\alpha^3 |\lambda| (-1)^{x+x'} (\delta_{q',q} [1 + (-1)^{y+y'}] + \\ &+ \text{sign}(\lambda) [\delta_{q',q-1} (-1)^{y'} + \delta_{q',q+1} (-1)^y]). \end{aligned} \quad (16)$$

An interesting feature of this result is that for $q = q'$, *i.e.* for different chains of the same kind, $\mathbf{S}_{q,y}(\mathbf{x}) \cdot \mathbf{S}_{q,y'}(\mathbf{x}') \sim [1 + (-1)^{y+y'}]$. That is, spins from the like chains of opposite parity (when $y + y' = \text{odd}$) are orthogonal to each other. This peculiar feature of the cuboc order is clearly seen in panels (a) and (b) of Fig. 9. Note also that while the same-chain spin correlations are not sensitive to the sign of λ , those between the spins with different q 's are proportional to λ , and take opposite values in cuboc1 and cuboc2 phases. This feature too is visible in the numerical data of Fig. 9.

Spin chirality can be analyzed similarly. We find

$$\begin{aligned} \mathbf{S}_{1,y_1}(\mathbf{x}_1) \cdot \mathbf{S}_{2,y_2}(\mathbf{x}_2) \times \mathbf{S}_{3,y_3}(\mathbf{x}_3) &= (2\alpha^3 |\lambda|)^{3/2} (-1)^{x_1+x_2+x_3} \\ &\times [\text{sign}(\lambda) + (-1)^{y_1+y_2+y_3}] \hat{\mathbf{e}}_1 \cdot \hat{\mathbf{e}}_2 \times \hat{\mathbf{e}}_3. \end{aligned} \quad (17)$$

This shows that chiralities $\chi_{\Delta_1, \Delta_3, \Delta_4}$ acquire finite (and different) expectation values in the two cuboc phases, see Fig. 10. At the same time within the chain mean-field $\chi_{\Delta_2} = 0$ because it involves two spin from the same chain, which nullifies the triple product of spins identically. Numerical data in Fig. 10 does show somewhat suppressed but certainly not zero χ_{Δ_2} . This, we think, happens due to contributions from the subleading uniform part $\tilde{\mathbf{M}}_{q,y}(\mathbf{x})$ of the spin operator, Eq. (3), which is not captured by the mean-field treatment.

The chain mean-field approach completely neglects *marginal* interchain interaction of spin currents, $4J_1 \sum_{y,y'} \mathbf{M}_{q,y}(-y') \mathbf{M}_{q+1,y'}(y+y')$, see Eq. (6). This approximation is truly justified only in the weak coupling $J_{1,2} \ll J_d$ limit, when the logarithmically slow growth of the marginal coupling constant (scaling dimension 2) is certain to *not* spoil an exponentially faster growth of the relevant $\mathbf{N}_q \cdot \mathbf{N}_{q+1}$ term (scaling dimension 1). However, a ferromagnetic (negative) sign of the interchain interactions $J_{1,2}$ is known to change this marginal interaction into a marginally irrelevant (logarithmically decaying) one, which has the effect of extending the range of validity of the chain mean-field approximation [41].

2. Compensated regime

Near the line $J_1 = J_2$, the leading coupling λ vanishes. Here it is necessary to include the subdominant term in Eq. (6). Owing to the derivative and the factor of $\mathbf{M}_{q,y}$, it appears to be strongly irrelevant, and naively one might expect

that the decoupled chain state is stable. In reality, it generates a more subtle instability towards VBC order. This occurs by a fluctuation effect: the irrelevant coupling in Eq. (6) generates a relevant one at second order upon renormalization.

The procedure for calculating this fluctuation correction was worked out in Ref. 39. We work with the imaginary time path integral and expand the weight e^{-S} to second order in the interaction part of the action $S' = \int d\tau H'|_{\text{sub-dom}}$, and use the fusion rules of the current algebra of $SU(2)_1$ to per-

form the renormalization. The correction to the effective action is

$$\delta S = -\frac{1}{2} \int d\tau d\tau' [H'|_{\text{sub-dom}}(\tau) H'|_{\text{sub-dom}}(\tau')]_>, \quad (18)$$

where the brackets $[\cdot]_>$ indicates renormalization by removing of high energy/short-time degrees of freedom. The dominant effect comes from the cross-term,

$$\begin{aligned} \delta S &\sim -\frac{(J_1)^2}{2} \sum_{y,y',q} \int d\tau d\tau' \left[\left(2M_{q,y}(-y',\tau) + (-1)^{y'} \partial_x N_{q,y}(-y',\tau) \right) \cdot \left(2M_{q+1,y'}(y+y',\tau) + (-1)^{y+y'} \partial_x N_{q+1,y'}(y+y',\tau) \right) \right. \\ &\quad \times \left. \left(2M_{q,y}(-y',\tau') + (-1)^{y'} \partial_x N_{q,y}(-y',\tau') \right) \cdot \left(2M_{q+1,y'}(y+y',\tau') + (-1)^{y+y'} \partial_x N_{q+1,y'}(y+y',\tau') \right) \right]_> \\ &= -\frac{(J_1)^2}{2} \sum_{a,b=x,y,z,y,y',q} \int d\tau d\tau' \left[\left(2M_{q,y}^a(-y',\tau) + (-1)^{y'} \partial_x N_{q,y}^a(-y',\tau) \right) \left(2M_{q,y}^b(-y',\tau') + (-1)^{y'} \partial_x N_{q,y}^b(-y',\tau') \right) \right]_> \\ &\quad \times \left[\left(2M_{q+1,y'}^a(y+y',\tau) + (-1)^{y+y'} \partial_x N_{q+1,y'}^a(y+y',\tau) \right) \left(2M_{q+1,y'}^b(y+y',\tau') + (-1)^{y+y'} \partial_x N_{q+1,y'}^b(y+y',\tau') \right) \right]_> \end{aligned} \quad (19)$$

We use the identity, from Eq. (35) of Ref. 39,

$$\left[M^a(x,\tau) \partial_x N^b(x,\tau') \right]_> = -\frac{\delta^{ab} \varepsilon(x,\tau)}{2\pi v^2 (\tau - \tau' + \tau_0 \sigma_{\tau-\tau'})^2}, \quad (20)$$

where $v = \pi J_d/2$ is the velocity of the 1d Heisenberg chain, $\tau_0 \sim 1/J_d$ is a short-time cutoff, and $\sigma_\tau = \text{sign}(\tau)$. Using this gives

$$\begin{aligned} \delta S &\sim -8J_1^2 \sum_{a,b} \sum_{y,y',q} \int d\tau d\tau' (-1)^y \frac{\delta^{ab} \varepsilon_{q,y}(-y',\tau)}{2\pi v^2 (\tau - \tau' + \tau_0 \sigma_{\tau-\tau'})^2} \frac{\delta^{ab} \varepsilon_{q+1,y'}(y+y',\tau)}{2\pi v^2 (\tau - \tau' + \tau_0 \sigma_{\tau-\tau'})^2} \\ &= -\frac{24J_1^2}{(2\pi)^2} \sum_{y,y',q} \int d\tau \left[\int d\tau' \frac{1}{(v\tau' + \tau_0 v \sigma_{\tau'})^4} \right] (-1)^y \varepsilon_{q,y}(-y',\tau) \varepsilon_{q+1,y'}(y+y',\tau) \\ &= -\frac{4J_1^2}{\pi^2 v a_0^3} \sum_{y,y',q} \int d\tau (-1)^y \varepsilon_{q,y}(-y',\tau) \varepsilon_{q+1,y'}(y+y',\tau), \end{aligned} \quad (21)$$

where $\tau_0 v = a_0$ is a short-distance cut-off. This can be interpreted as the integral of a correction to the Hamiltonian,

$$\delta H_{\text{int}} = -\frac{4J_1^2}{\pi^2 v a_0^3} \sum_{y,y',q} (-1)^y \varepsilon_{q,y}(-y') \varepsilon_{q+1,y'}(y+y'). \quad (22)$$

Note the distinct similarity to Eq. (4), with staggered dimerization ε replacing the Néel operator N .

The interaction δH_{int} should be added to that in H'_{dom} . For $J_1 = J_2$, it becomes the only important interaction. We analyze it using chain mean field theory, as we did for the dominant interaction away from this line above. We write the variational Hamiltonian

$$\tilde{H}_{\text{var}} = H_0 - \sum_{q,y} \int d\mathbf{x} \varphi_{q,y} \varepsilon_{q,y}(\mathbf{x}). \quad (23)$$

We have $\tilde{\varepsilon}_{q,y} = \langle \varepsilon_{q,y} \rangle = \tilde{\alpha} |\varphi_{q,y}|^{1/3} \text{sign}(\varphi_{q,y})$, with $\tilde{\alpha} > 0$ an-

other $O(1)$ constant, and the variational energy is

$$\tilde{E}_{\text{var}} = \frac{L}{4\tilde{\alpha}^3} \sum_{q,y} \tilde{\varepsilon}_{q,y}^4 - \tilde{\lambda} \sum_q \sum_{y,y'} (-1)^y \tilde{\varepsilon}_{q,y} \tilde{\varepsilon}_{q+1,y'}. \quad (24)$$

Here we defined $\tilde{\lambda} = 4J_1^2/(\pi^2 v a_0^3)$. Now define

$$V_q = \frac{1}{L} \sum_y (-1)^y \tilde{\varepsilon}_{q,y}, \quad W_q = \frac{1}{L} \sum_y \tilde{\varepsilon}_{q,y}. \quad (25)$$

Then the energy becomes

$$\tilde{E}_{\text{var}}/L = \frac{1}{24\tilde{\alpha}^3} \sum_q [(V_q + W_q)^4 + (V_q - W_q)^4] - \frac{\tilde{\lambda}}{3} \sum_q V_q W_{q+1}. \quad (26)$$

All these manipulations and formulae look very similar to those we carried out for magnetic ordering, but the minima

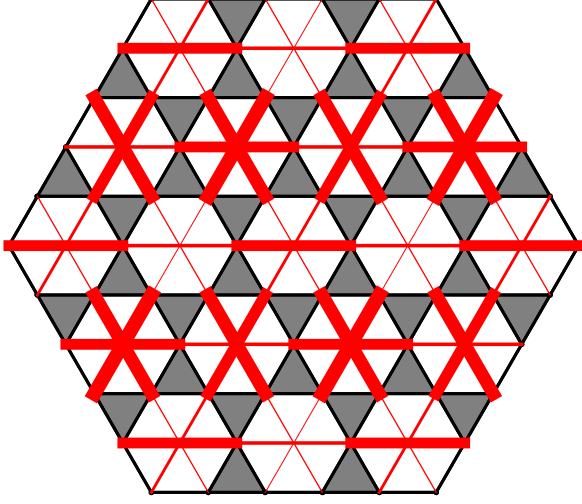


FIG. 4: (Color online) Analytically predicted VBC pattern in two dimensions. The thickness of each red line is proportional to the magnitude of the exchange on the bond. Observe that the unit cell is quadrupled. This pattern may be compared to the one obtained by the DMRG calculation in Fig. 13(a).

of the variational energy are quite different. This is because $\bar{\epsilon}$ is a scalar, and as a consequence the ordering is more frustrated. Some algebra shows that the global minima of Eq. (26) are of the form

$$\begin{aligned} (V_1, V_2, V_3) &= \sqrt{\tilde{\alpha}^3 \tilde{\lambda}} (0, sv, s'(v')^3), \\ (W_1, W_2, W_3) &= \sqrt{\tilde{\alpha}^3 \tilde{\lambda}} (s'v', 0, s(v)^3), \end{aligned} \quad (27)$$

where $v = (7+3\sqrt{5})^{1/8}/\sqrt{2} \approx 0.981$ and $v' = (7-3\sqrt{5})^{1/8}/\sqrt{2} \approx 0.606$, or vice-versa, and s and s' are independently and freely taken to be ± 1 , and finally, the solution in Eq. (27) can also be cyclically permuted, $V_q \rightarrow V_{q+1}, W_q \rightarrow W_{q+1}$. This gives a set of 24 minima with equivalent energy, $\tilde{E}_{\text{var}} \approx -0.18\tilde{\alpha}^3 \tilde{\lambda}^2$. The corresponding order is illustrated in Fig. 4. By working out the action of the space group symmetry of the kagomé lattice (see Appendix A), we can check that all these 24 states are related by symmetry. So this degeneracy is not accidental and is mandated.

3. Phase boundaries

Based on the above discussion, we expect the VBC phase on the line $J_1 = J_2$, and the two cuboc phases away from this line. Since the VBC state is a *phase*, it must exist in a finite width region around the compensated line. The shape of the boundaries of this region is determined by comparing the VBC and magnetic coupling constants, because the interactions in Eq. (4) and Eq. (22) have the same scaling dimension. This means the boundaries occur when comparing Eqs. (14) and (27), $\sqrt{|\lambda|} \sim \sqrt{\tilde{\lambda}}$. Equivalently, we can compare the energies of the two orders, $E_{\text{var}} = \tilde{E}_{\text{var}}$. Approx-

imating the ratio $\alpha/\tilde{\alpha} \sim 1$ and using $\nu a_0 = \pi J_d/2$, we obtain

$$\frac{J_1}{J_d} - \frac{J_2}{J_d} = \pm 0.055 \left(\frac{J_1}{J_d} \right)^2. \quad (28)$$

This is only a scaling relation – the numerical prefactor above is an estimate based on a weak-coupling analysis. Its smallness would imply a region of VBC phase narrower than the DMRG numerics of Sec. III would indicate, suggesting the true prefactor may be larger. However, Eq. (28) is enough to show that the VBC phase occupies a wedge-shaped region around the diagonal in the $J_1 - J_2$ plane, which pinches down to zero width as the origin is approached, as is sketched in the phase diagram in Fig. 2.

C. Cylinders

To compare with DMRG calculations on finite circumference (L_y) cylinders, we consider this type of geometry explicitly. In general, a complicated dependence may exist on the choice of embedding the lattice into the cylinder, and also the cylinder circumference. For small cylinders, the finite size effects can be quite substantial. This is especially expected when there is a long length scale already in the two dimensional problem, for example in the limit $J_1, J_2 \ll J_d$. Then we need to compare the circumference to this two dimensional correlation length.

1. Quasi-2d limit

In the limit of very large circumference cylinders, i.e. when the circumference is large compared to all two dimensional correlation lengths, then we expect relatively universal behavior. In this case, the system is essentially ordered on scales smaller than the cylinder width, and the only important degrees of freedom on those scales and larger are captured by the order parameter(s). We will call this the quasi-2d limit.

If the two dimensional system is in one of the magnetically ordered cuboc states, then there are two order parameters. One is the discrete chiral order parameter, which is of Ising type. The other is the continuous SO(3) order parameter that specifies the specific spin orientations. The former chiral order parameter has only gapped fluctuations, and would be expected can retain its order at $T = 0$ in the limit of wide cylinders, even as the length of these cylinders extends to infinity. So we expect *spontaneous chiral order in sufficiently wide cylinders away from the compensated line*. The SO(3) order parameter, being continuous, by contrast cannot spontaneously order in one dimension. It instead is governed by an SO(3) matrix non-linear sigma model in 1+1 dimensions with a small coupling constant $g \sim 1/L_y$ (effective “temperature” for 2d Euclidean theory), which is expected to be asymptotically free. Some gapped behavior, with exponentially decaying spin correlations beyond some *one-dimensional* correlation length $\xi_{1d} \sim \exp(g_0/g)$ should be expected. This may be accompanied by spontaneous

dimerization, whose presence may depend upon the parity of the circumference.

This argument also suggests that for sufficiently small L_y (that is, high effective temperature) the chiral order will melt as well, leading to a state without long range order in both spin and chiral degrees of freedom. This is perhaps what is observed in cuboc regions in both XC and YC geometries (see the definitions in Fig. 7), see Figs. 10 and 12, panels (c) and (d).

In the vicinity of the compensated line, we expect VBC order in the infinite 2d limit. Since the VBC phase has an entirely discrete order parameter, we expect symmetry breaking to remain for finite width cylinders. The analysis is involved, however, since the symmetries broken by the VBC order are space group operations, some of which are broken by confinement to the cylinder, in ways which depend upon the geometry and circumference of the cylinder. A further complication is that, for some cylinders, notably of odd circumference, the 2d VBC order may be incompatible with periodic boundary conditions around the cylinder. In this case, defects such as domain walls may be present, and the gap may close at these defects. We will eschew any detailed analysis beyond these general remarks.

2. Quasi-1d Limit: YC cylinders

If the cylinder circumference is not too large, it can interfere with even the short-range development of order. The effect is particularly clear for the YC cylinders, in which one of the three types of chains – we choose this to be type “1” for concreteness – is oriented along the periodic direction. The type 1 chains are therefore finite in the YC geometry. For such finite chains, even without any inter-chain coupling, the spins form a gapped singlet state, with a gap of order ν/L_y . We can expect that if the inter-chain coupling is in some sense weaker than this finite size gap, the spins on these chains will resist ordering.

At a first level of analysis, we can understand the physics of this limit by simply neglecting the type 1 spins. Dropping the $N_{q,y}$ terms in Eq. (4), we obtain unfrustrated interactions between the Néel fields on the remaining chains type 2 and 3 chains, which actually favors *collinear* ordering. This is also apparent from a visual inspection of the geometry of the 1-2 sublattices alone (see Fig. 5). One observes that a ferromagnetic J_1 interaction is unfrustrated and results in ferromagnetic alignment of spins in each vertical column, with successive columns aligned antiferromagnetically, due to the strong antiferromagnetic J_d coupling. In this pattern all J_1 and J_d interactions are perfectly satisfied. A ferromagnetic J_2 induces instead ferromagnetic alignment of each horizontal row of spins, with antiferromagnetic alignment of successive rows by J_d . Here all J_2 and J_d interactions are satisfied.

The conclusion is that for the YC cylinders of “small” circumference, there is a strong finite size effect which favors *collinear* order rather than the non-collinear cuboc type. Spins on the type 1 chains are gapped by finite size ef-

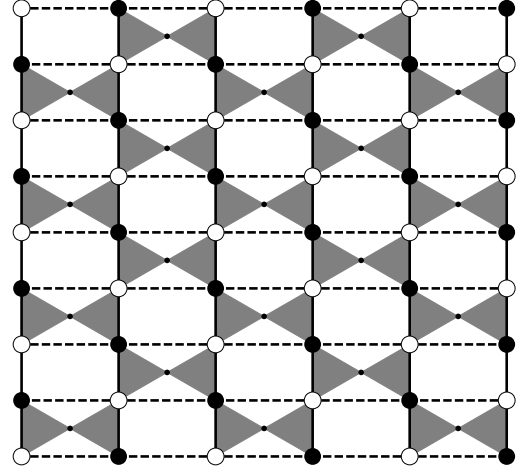


FIG. 5: Two types of gapless chains in the YC cylinder geometry, and their couplings. White and black circles represent the sites of two types of infinite chains. Solid vertical bonds and dashed horizontal ones are the J_1 and J_2 couplings between these sites.

fects, and exhibit exponential decay of correlations along the cylinder with a correlation length of order a single lattice site. In either collinear pattern the net exchange field on the type 1 sites vanishes, so there is no induced moment there. The collinearity and absence of a moment on the type 1 site means that the chirality is suppressed, and should exhibit exponential correlations along the cylinder, similar to that of the type 1 spins, and even further suppressed by the collinearity of the type 2+3 spins.

For a very long cylinder of finite circumference, the chain mean field theory must be further corrected for one-dimensional quantum fluctuations. This of course prohibits any type of, including collinear, Néel long range order. Instead the system will be governed by a vector SO(3) nonlinear sigma model, and we expect only a trivial Θ term for the even circumference cylinders we study here. Ultimately this will induce a small gap and exponential decay of correlations also on the type 2 and 3 sites, but with a much longer correlation length. However, on observable short distances we expect to observe behavior quite compatible with two dimensional Néel orders of the types indicated above. The data in the “magnetically ordered” regime from the DMRG on YC cylinders fits very well to such collinear behavior for small circumference, as Fig. 11 shows.

VBC state in the YC cylinder: On the compensated line $J_1 = J_2$, we again need to consider the fluctuation-induced dimerization interactions of Eq. (22), but now examine its effects on the finite cylinder. Due to the smaller magnitude of the induced dimerization coupling, the finite size effects on the short type 1 chains is even more significant – the finite size gap is larger relative to this interaction. Hence in this geometry, we should simply neglect dimerization of the type one chains, and set $\bar{\epsilon}_{1,y} = 0$. Then the minimum of the chain mean field variational energy is simply

$$V = \sqrt{\bar{\alpha}^3 \bar{\lambda}}(0, s, 0), \quad W = \sqrt{\bar{\alpha}^3 \bar{\lambda}}(0, 0, s), \quad (29)$$

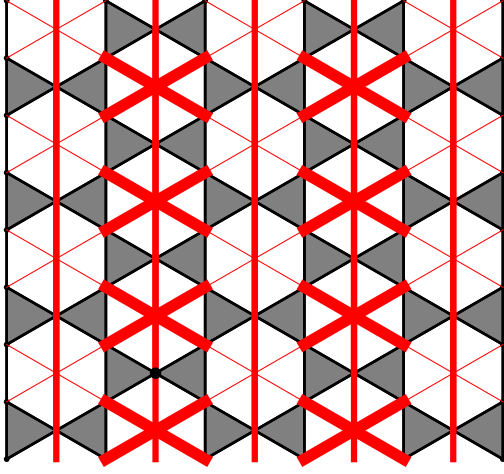


FIG. 6: The analytically predicted VBC state on YC cylinders, which differs from that in Fig. 4 due to strong finite size effects. This should be compared to the DMRG result in Fig. 13(b).

with $s = \pm 1$ defining two degenerate solutions. The resulting VBC pattern, shown in Fig. 6, is translationally invariant in the vertical (1) direction along the cylinder circumference, and has period two normal to it. The two signs of the solution simply represent these translational copies. Note that the strong finite size effects have greatly simplified the VBC order relative to the 24-fold degenerate state expected in two dimensions. The DMRG results for YC cylinders at $J_1 = J_2$ seems most consistent with this simpler VBC order, see Fig. 13(b).

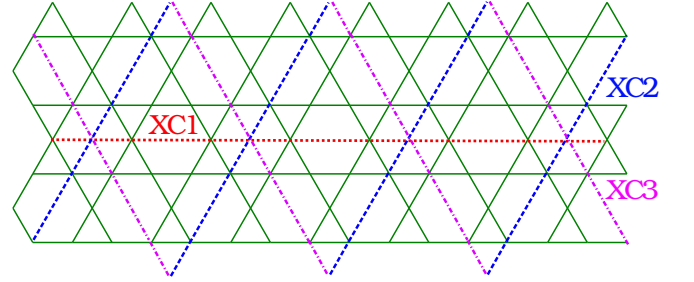
The presented arguments make us conclude that XC cylinders, results on which are described in details in the next section, approximate the desired 2d limit of the model better than those of YC kind. Nonetheless the seemingly exponential decay of the chirality correlations in Fig. 10, panels (c) and (d), suggests that the studied XC cylinders are still too narrow to truly capture the 2d physics of the non-coplanar cuboc phase.

III. DMRG RESULTS

Here we report results of the numerical density-matrix renormalization group [42] (DMRG) studies of the $J_1 - J_2 - J_d$ kagomé model. Through calculations on cylinders, we establish the quantum phase diagram as shown in Fig. 2, which has two cuboctohedral phases, cuboc1 and cuboc2, separated by a VBC phase region. We use a DMRG algorithm with spin rotational $SU(2)$ symmetry [43] by keeping a number of $U(1)$ -equivalent states as large as 32000. To mitigate and understand finite size effects, we study two different cylinder geometries denoted as XC and YC, which have one of the three bond orientations along the x and y axes, respectively (see Fig. 7). The system size is denoted as $XC2L_y - L_x$ and $YC2L_y - L_x$, where L_y (L_x) is the number of unit cells in the y (x) direction. We study the YC cylinders

with $L_y = 4, 6$ (YC8 and YC12) and XC cylinders with $L_y = 4$ (XC8). We do not study the XC12 cylinder ($L_y = 6$), because this geometry does not accommodate the cuboc ordering pattern. For the XC8 and YC8 cylinders, we obtain the converged energy with DMRG truncation error $\sim 1 \times 10^{-6}$ by keeping about 16000 $U(1)$ -equivalent states. For the YC12 cylinder, the truncation error can only be reduced to about 5×10^{-5} . Although the calculations are not well converged for the YC12 cylinder, the results for this system are qualitatively consistent with those for the YC8 cylinder.

(a) XC8-8 cylinder



(b) YC8-8 cylinder

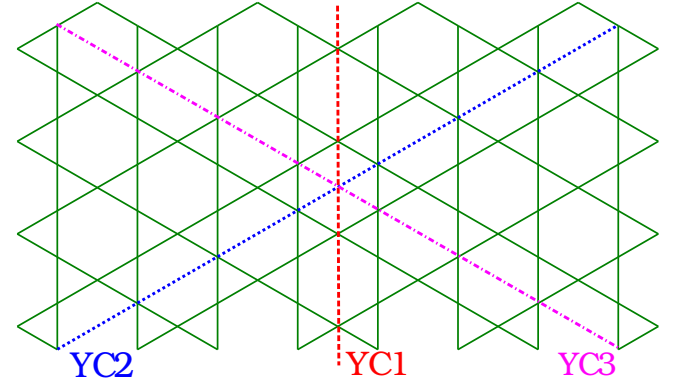


FIG. 7: (Color online) Cylinder geometries used in the DMRG calculations. (a) A XC8-8 cylinder on kagomé lattice. This cylinder has 4 unit cells along the y direction and 8 unit cells along the x direction. The three dashed lines denote the J_d chains along the three directions. This cylinder has 4 XC1 chains with 8 sites along the x direction and 2 XC2 and XC3 chains with 16 sites along the tilted directions. All the J_d chains are extended, i.e. have a length proportional to the long dimension of the cylinder. (b) A YC8-8 cylinder on kagomé lattice. This cylinder has 4 unit cells along the y direction and 8 unit cells along the x direction. The three dashed lines denote the J_d chains along the three directions. This cylinder has 9 YC1 chains with 4 sites along the y direction and 4 YC2 and YC3 chains with 8 sites along the tilted directions. While the YC2 and YC3 chains are extended, the YC1 chains are closed with a short circumference along the y direction.

To obtain a coarse understanding of the phase diagram, we calculate and compare the magnetic structure factor $S(\mathbf{k}) = \frac{1}{N} \sum_{i,j} e^{i\mathbf{k} \cdot (\mathbf{r}_i - \mathbf{r}_j)} \langle \mathbf{S}_i \cdot \mathbf{S}_j \rangle$ in different parameter regions for the XC cylinders. We define the Brillouin zone based on an extended triangular lattice in real space [31], which has a virtual site in the center of each hexagon of the kagomé lattice. We define the lattice spacing in real space as the near-

est J_1 bond length. Thus in the plots in Fig. 8, which show representative structure factors, the smaller white hexagon is the Brillouin zone of the kagomé lattice and the larger one is the Brillouin zone of the extended triangular lattice. The dashed blue lines denote the momentum space of the decoupled one-dimensional J_d chains. When calculating the structure factor, the spin correlations including the virtual sites are all set to zero.

Fig. 8(a) shows the structure factor for $J_1 = J_2 = 0$, in which the system consists of decoupled chains. In this case it exhibits peaks at the momenta with $\mathbf{k} \cdot \mathbf{a}_q = \pi$ (the \mathbf{a}_q with $q = 1, 2, 3$ were defined in Sec. II A). One can observe that the peak momenta are the crossing points of the momentum lines. The remaining three plots, Figs. 8(b,c,d) show the structure factor with non-zero interchain coupling. Notably, in all cases, the peaks of the structure factor coincide some subset of those of decoupled chains, which indicates the appropriateness of the treatment of the system in Sec. II. In the compensated region with $J_1 \approx J_2$, Fig. 8(b), all the features of the decouple chain structure factor are preserved – both high intensities along lines and peaks at their intersections. However, the features themselves are broadened, and the structure factor appears much less singular. This suggests the system remains a liquid as in the decoupled chains case, but with short-range rather than power law spin correlations. In the parameter region far from the compensated line $J_1 = J_2$, we find that, as shown in Figs. 8(c,d), the peaks of $S(\mathbf{k})$ locate at the six inner crossings or at the outer crossings depending for $|J_1| > |J_2|$ or $|J_1| < |J_2|$, respectively. The selection of the inner and outer points agrees with the cuboc phases as shown in the insets of Fig. 1. One further observes in Figs. 8(c,d) that two of the six peaks have larger intensity, which must be attributed to the rotational symmetry breaking induced by the cylindrical geometry. This physics is discussed in Sec. II C 2, and we return to it in Sec. III A 2. We now discuss the DMRG results in detail for each phase region.

A. Magnetically ordered region

First of all, we study the phase regions with the cuboc-like magnetic structure factors, which are far from the compensated line $J_1 = J_2$.

1. XC cylinders

Fig. 7(a) shows the geometry of the XC8-8 cylinder, and the labeling for three types of chains, indicated by dashed lines. Chains XC2,3 are seen to wind around the cylinder while chains XC1 run parallel to the cylinder's axis. In this geometry all chains are long, i.e. proportional to the cylinder length, which helps to reduce finite-size effects. Fig. 9 shows the real space spin correlations for the XC8-36 cylinder. When the reference spin, which is shown by a green circle, belongs to chain XC1 (Figs. 9(a-b)), its correlations with the spins from the *same* XC1 chain are staggered in an an-

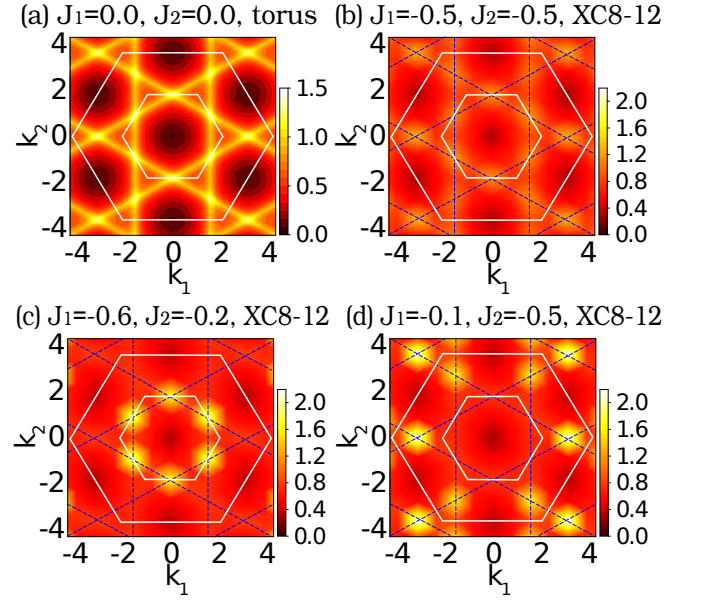


FIG. 8: (Color online) Magnetic structure factor $S(\mathbf{k})$ in the extended Brillouin zone of the extended triangular lattice. The lattice spacing in real space is the length of the J_1 bond. (a) $S(\mathbf{k})$ of the decoupled J_d chains ($J_1 = J_2 = 0.0$) on the $N = 3 \times 12 \times 12$ torus. (b)-(d) $S(\mathbf{k})$ obtained on XC8-12 cylinder for different phases. The blue dashed lines denote the momenta of the decoupled J_d chain system. In the compensated regime (b), $S(\mathbf{k})$ has the peaks at the same momenta as the decoupled J_d chains as shown in (a), but is much smoother. In the cuboc2 phase (c), the peak intensity of the structure factor is at the six inner crossings, while in the cuboc1 phase (d), it is at the outer line crossings. Due to the anisotropy inherent to the cylinder geometry, the magnitude of the six peaks of $S(\mathbf{k})$ are different.

tiferromagnetic Néel pattern. The same is true for the *next-nearest* XC1 chains. Note, however, that correlations with the spins from the *nearest* XC1 chains are essentially absent. This is in full agreement with the $[1 + (-1)^{y+y'}]$ structure of the correlations discussed below Eq. (16). This in particular is indicative of the cuboc states, in which spins on successive chains are orthogonal – see Fig. 1. In addition, correlations between spins on XC1 chain and those on the neighboring sites belonging to XC2 chain and XC3 chain are seen to change sign in going from the $\lambda = 2(J_1 - J_2) > 0$ phase, Fig. 9(a), to the $\lambda < 0$ one, Fig. 9(b). This too is in agreement with Eq. (16). In Figs. 9(c-d), we show the spin correlations with the reference spins on XC3 chain, which exhibit similar cuboc-like magnetic correlations.

To investigate whether the cuboc states have developed long-range magnetic order, we study the distance dependence of spin and chiral correlations. In Figs. 10(a-b), we plot the spin correlations along the three J_d chains, as a function of the distance along the chains, x , for two systems in the cuboc1 (a) and cuboc2 (b) regimes. For comparison, the correlations for a single isolated Heisenberg chain is also shown. We see that the spin correlations agree with those of the Heisenberg chain at short distance $x \leq 2$, but are enhanced significantly above them (note the logarith-

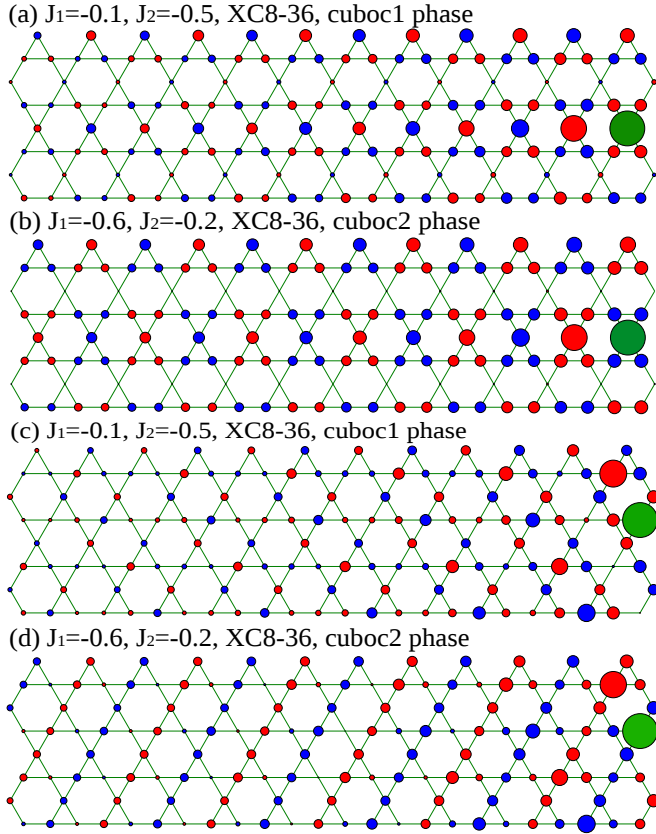


FIG. 9: (Color online) Spin correlation functions in real space on the XC8-36 cylinders. Panels (a) and (b) show the correlations with a reference sites on the XC1 chain. Panels (c) and (d) show the correlations with a reference site on the XC3 chain. The green site denotes the reference site in the middle of cylinder. The blue and red circles denote the positive and negative correlations, respectively. The magnitudes of correlation is proportional to the area of the circle.

mic scale) for larger x . This is a strong indication that the system is long-range ordered in the 2d limit. Despite the enhancement, the spin correlations due continue to decay, albeit slowly, with distance, rather than saturation. We attribute this to the inevitable 2d to 1d crossover which occurs for a quasi-one-dimensional system. In fact, for any finite width cylinder, *exponential* decay of the spin correlations is expected at sufficiently large L , due to one-dimensional fluctuations at low energy – see Sec. II C 1. The fact that the decay is relatively weak is a strong indicator that the underlying two-dimensional state is long-range ordered, rather than a gapless spin liquid behavior [36].

The cuboc states spontaneously break time-reversal symmetry and are characterized by finite scalar chirality $\langle \chi_{\Delta_i} \rangle \neq 0$, where $\chi_{\Delta_i} = (\mathbf{S}_{i,1} \times \mathbf{S}_{i,2}) \cdot \mathbf{S}_{i,3}$ and $\mathbf{S}_{i,m}$ ($m = 1, 2, 3$) are the three spins forming triangle Δ_i ($i = 1, 2, 3, 4$) shown in the inset of Fig. 10(d). The distance dependence of the chiral-chiral correlations $\langle \chi_{\Delta_i} \chi_{\Delta_j} \rangle$ for each of the four kinds of smallest triangles are plotted in Figs. 10(c-d).

For the cuboc1 state, we expect that the three-spin scalar chiral order of the triangles Δ_3, Δ_4 are non-zero and that for

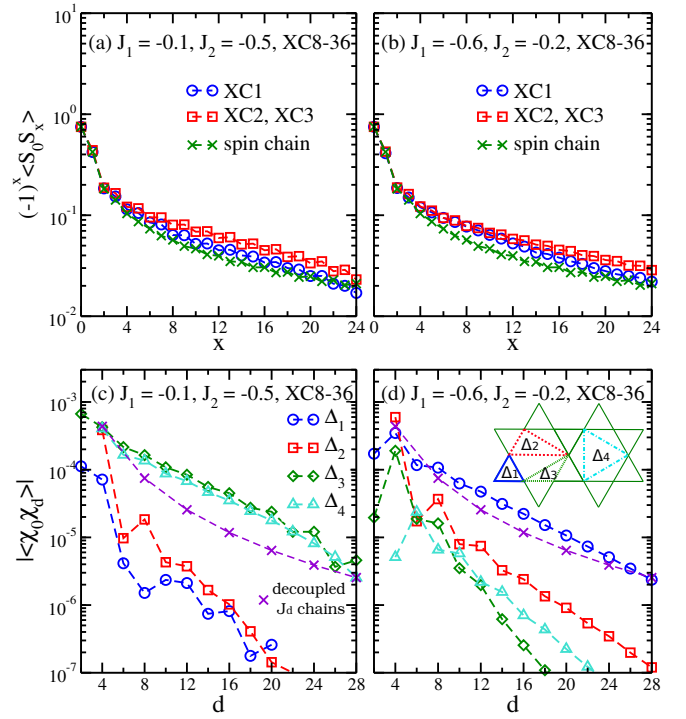


FIG. 10: (Color online) Log-linear plot of the correlation functions on the XC8-36 cylinder. Panels (a) and (b) give the spin correlations along the different J_d chain directions as shown in Fig. 7(a). Note that the spin correlations are enhanced above those of an isolated Heisenberg chain, plotted for comparison. Panels (c) and (d) give the chiral correlations of different types of triangles, versus the distance d along the x direction. The definition of the different triangles is shown in the inset of (d). The triangles which would have non-zero chirality in the appropriate classical cuboc state show chiral correlations enhanced above those of independent Heisenberg chains, while those whose chirality vanishes in the classical state have chiral correlations suppressed below the decoupled chain value.

Δ_1, Δ_2 vanish, which for the cuboc2 state, we expect only Δ_1 has non-vanishing chirality [20, 35]. The chiral correlations on the XC8 cylinder are presented in Figs. 10(c-d). Indeed, panel (c) shows that the chiralities which vanish in the cuboc1 ordered state are extremely small in the $|J_2| > |J_1|$ region, vanishing rapidly with distance and taking values close to the precision of the calculation. The same holds for the chiralities which are expected to vanish in the cuboc2 state for $|J_1| > |J_2|$, as shown in panel (d). In either case, the chiralities which would be expected to be non-zero in the ordered system still decay exponentially, but are substantially larger. The relative magnitudes of the various chiralities are indicative of cuboc states. For comparison, we show the chiral correlations of triangle types 1, 3, and 4 for decoupled J_d chains. One observes that this lies between than of the strong and weak chiralities in the cuboc regimes, again indicative of ordered behavior. However, the apparent exponential decay of the larger chiralities is *not* expected in the fully quasi-2d limit – see Sec. II C 1. This indicates that there are still finite size effects due to insufficiently large

L_y . We note that the relatively small magnitude of the chirality correlations can be understood simply from the fact that it is a three-spin operator, residing on three different chains. Roughly speaking, therefore, the chirality correlations should have a similar magnitude to the short-distance correlations of the spins *cubed*. This is generally in accord with the data.

2. YC cylinders

In the YC geometry, two of the chains YC2 and YC3 winding around the cylinder while the chains of YC1 kind run along the periodic y direction and are rather short, containing only 4 or 6 sites for YC8 and YC12 cylinders, respectively.

According to the analytical discussion in Sec. II C 2, the short YC1 chains are strongly gapped which has the effect of strongly suppressing chiral spin order and non-coplanar spin correlations associated with it. In Fig. 11 we present the spin correlations with a reference spin on a YC3 chain. The similarity of the data with the predicted collinear spin pattern in Fig. 5 is striking. The reference spin in Fig. 11 has strong correlations with the spins on YC2 and YC3 chains, but very weak correlations with those on the YC1 chains, consistent with the proposed large gap formation. In addition, the observed ‘striped’ ordering – ferromagnetic ordering along horizontal/vertical directions in cuboc1/cuboc2 phases – is also fully consistent with simple arguments in Sec. II C 2.

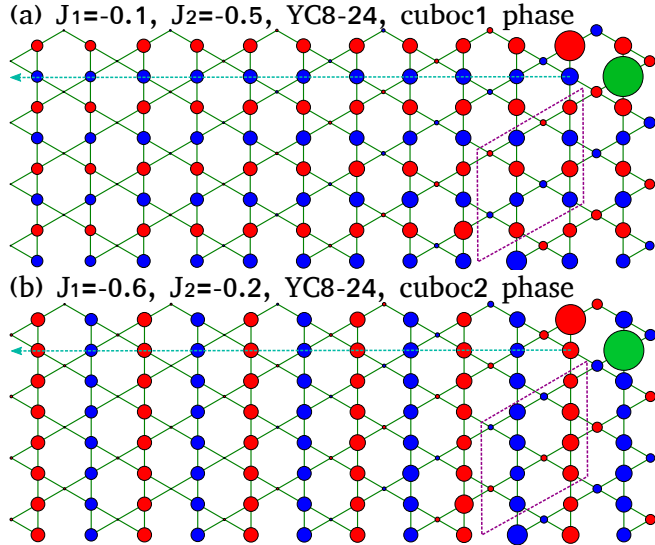


FIG. 11: (Color online) Spin correlation functions in real space on the YC8-24 cylinders. The green site is the reference spin in the middle of cylinder. The blue and red circles denote the positive and negative correlations, respectively. The magnitudes of correlations are proportional to the area of circle. The dashed diamonds denote the 12-site unit cells.

The ‘gapping out’ of the YC1 chains relieves frustration (see Fig. 5) and therefore has the effect of enhancing correlations between spins from the YC2,3 chains. Our data in

Figs. 12(a-b) reflects this well. The observed slow decay of spin correlations with the distance, which is found to be robust with respect to increase in the number of kept DMRG states, strongly suggests collinear spin ordering. Correspondingly, and in agreement with our numerical findings, we find the chiral correlations to be strongly suppressed in this geometry, as is shown in Figs. 12(c-d). Together these results vindicate the conclusion that strong finite size effects on the YC cylinders studied completely change the ground state from an non-collinear to a collinear one in the magnetically ordered regions. We conclude that the YC cylinders do not give behavior representative of the two dimensional limit. However, the consistency with theory shows that we have an excellent control over finite size effects using the quasi-1d analytical approach.

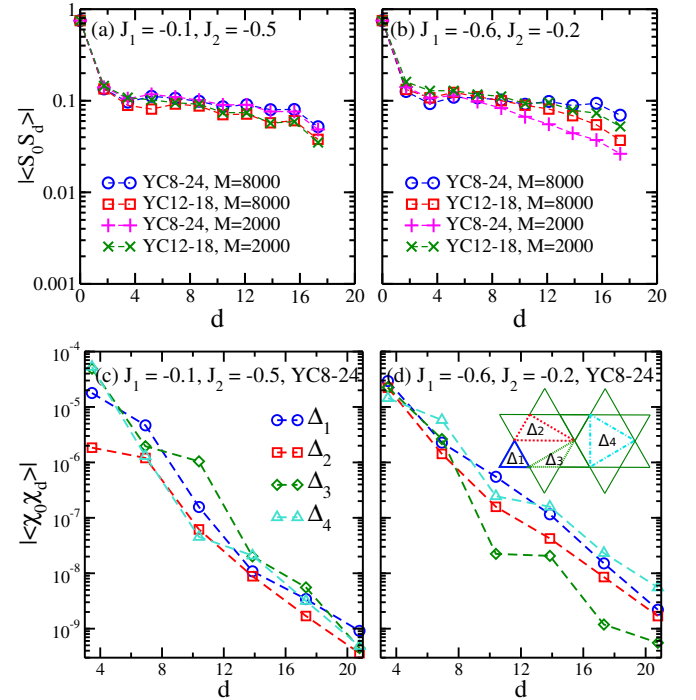


FIG. 12: (Color online) Log-linear plots of the correlation functions on the YC cylinders. Panels (a) and (b) show the spin correlations on the YC8-24 and YC12-18 cylinders along the dashed lines in Fig. 11. Panels (c) and (d) plot the chiral correlations versus the distance along the x direction on the YC8-24 cylinder.

B. VBC phase in the compensated regime

In the vicinity of the compensated line $J_1 = J_2$, our analytical studies find a VBC state as shown in Fig. 4 rather than a decoupled chain state. To detect the possible lattice translational symmetry breaking, we have calculated the bond energy pattern on both XC8 and YC8 cylinders, see Fig. 13. The observed dimerization pattern indicates an instability of the decoupled chain state towards a VBC under J_1, J_2 perturbations. On the XC8 cylinder, we find that a dimerization pat-

tern which is very compatible with the analytical result in two dimensions: compare the theoretical plot of Fig. 4 with Fig. 13(a). On the YC8 cylinder, the dimerization pattern also fully agrees with the simpler VBC pattern found in the short-YC1-chain limit: compare Fig. 6 and Fig. 13(b). The good agreement between the DMRG and analytical results indicates that the VBC state found analytically in Sec. IIB2 is indeed the ground state in the compensated regime.

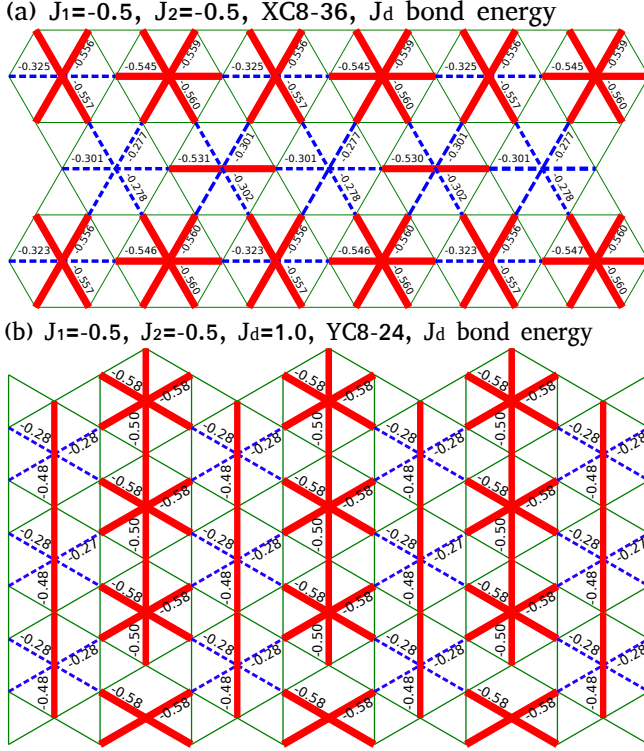


FIG. 13: (Color online) VBC pattern for $J_1 = J_2 = -0.5$ on (a) XC8-36 and (b) YC8-24 cylinders. The red solid and blue dashed lines denote the strong and weak J_d bond energy $\langle \mathbf{S}_i \cdot \mathbf{S}_j \rangle$ in the middle of cylinder. Panels (a) and (b) should be compared to the analytical predictions in Fig. 4 and Fig. 6.

C. Phase boundaries

In Sec. IIB3 we argued theoretically that the phase boundaries between the VBC and the cuboc phases have a wedge-like shape. To study the phase boundaries numerically, we calculated the dimer order parameter and the entanglement entropy on the XC8 and YC8 cylinders as a function of the J_1, J_2 couplings. As shown in Fig. 14, the J_d bond dimer order parameter is strongly peaked near the compensated line, indicating the VBC phase region. At the same time, we find that in the VBC region the entanglement entropy is strongly suppressed. The approximate phase boundaries extracted from these two independent quantities are well correlated with each other.

The VBC phase region obtained from DMRG calculations roughly agrees with the wedge-like shape of the dimer-

ized phase, sketched in Fig. 2, predicted analytically in the weakly-coupled chain limit. At the same time it is clear that the agreement is only qualitative as the width of the dimerized region found by DMRG is much wider than the analytical prediction Eq. (28). We attribute this discrepancy to the well-known fact that open ends of the spin chain induce finite staggered dimerization which decays slowly, $\propto L^{-1/2}$, towards the center of the chain of length L [44, 45]. This effect is of course most pronounced in the weakly-coupled limit $|J_{1,2}| \ll J_d$ (exactly where the discrepancy between numerical and analytical results is largest) where open-ended chain can be best viewed as having ‘pre-formed’ dimerization pattern – the main effect of interchain interactions $J_{1,2}$ is then to correlate phases of these ‘pre-formed’ patterns between different chains. The very fact that the symmetry of the resulting dimerization pattern, Figure 13, matches the analytical predictions, Fig. 4 and Fig. 6, implies that the over-estimate of the extend of the VBC region is only a quantitative, and not qualitative, feature of our DMRG study.

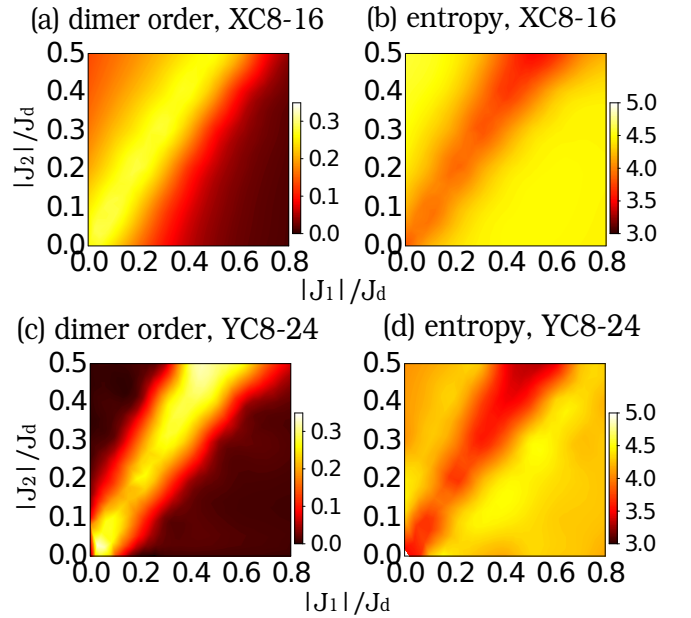


FIG. 14: (Color online) Coupling dependence of the bulk dimer order parameter and entanglement entropy on the XC8-16 and YC8-24 cylinders. (a) and (c) are the J_d bond dimer order parameter, which is defined as the difference between the strong and weak bond energy along the x axis. (b) and (d) are the bipartite entanglement entropy in the bulk of cylinder.

IV. CONCLUSIONS

A. Summary

Motivated by experiments on the kagomé antiferromagnet kapellasite [31], we have studied the spin-1/2 $J_1 - J_2 - J_d$ kagomé Heisenberg model (with ferromagnetic $J_1, J_2 < 0$, and antiferromagnetic $J_d > 0$ third-neighbor coupling

across the diagonal of the hexagon) in the J_d -dominant regime by using analytical and Density Matrix Renormalization Group (DMRG) calculations. This model has previously been argued to represent a good starting point for this material [31, 33, 34]. Both bosonic and fermionic parton constructions predicted chiral spin liquid phases in this model, in the regime relevant to kapellasite [31, 36, 46].

We approach the problem analytically by considering J_1 and J_2 as perturbations to J_d , i.e. formally $|J_1, J_2| \ll J_d$, so that the starting point consists of spin chains formed by strong J_d -bonds. We expect this to work so long as $|J_1|, |J_2|$ remain a fraction of J_d . Note that this domain of applicability includes most of the predicted range of the chiral spin liquid phases found in the most recent parton study [36]. We provide a controlled alternative. Utilizing a powerful field theory representation of the one-dimensional chains, we treat the weak J_1, J_2 bonds with the help of the systematic perturbative renormalization group method and a well-established chain mean field approximation.

For the parameter regimes away from the compensated line $J_1 = J_2$, this analysis predicts the non-coplanar cuboc1 and cuboc2 states with long-ranged magnetic order and finite scalar spin chirality. In the compensated regime with $J_1 \approx J_2$, the leading interchain interaction vanishes, and quantum fluctuations conspire to generate an effective four-spin interactions between chains, which is conveniently expressed in terms of interaction between dimerization densities from different spin chains. This new interaction promotes an interesting 24-fold degenerate Valence Bond Crystal (VBC) state which breaks lattice translational and rotational symmetries. We then extend this analysis to the cylinders of finite circumference and argue that the XC geometry minimizes finite size effects in comparison to the YC one.

In parallel with this, we carry out unbiased large-scale DMRG calculations for both the XC and YC cylinder systems. The DMRG results are summarized in the quantum phase diagram Fig. 2, which agrees well with the analytical predictions. We find cuboc1 ($|J_2| > |J_1|$) and cuboc2 ($|J_1| > |J_2|$) magnetic orders with scalar spin chirality based on the DMRG results on the XC cylinder. On the YC cylinder, all the chiral correlations decay extremely fast, in agreement with the analytical prediction that strong finite-size effects on the YC cylinder of small circumference relieve magnetic frustration and promote collinear Néel-like states over those with finite scalar chirality. The two magnetically ordered phases are separated by a spontaneously dimerized VBC state, whose structure is in excellent agreement with the analytical predictions. Like for the magnetically ordered region, the dimerization pattern is strongly affected by finite size effects in the YC geometry, but reflects the infinite 2d limit well in the XC cylinder.

B. Discussion

Our approach offers unexpectedly deep insight into the kagomé kapellasite problem. It demonstrates – for

the first time, to the best of our knowledge – emergent one-dimensional behavior of a structurally isotropic two-dimensional problem with hexagonal symmetry. Crucially, this emergent one-dimensionality *does not* imply spontaneous separation of the model into a collection of decoupled spin chains. Rather, it offers a valuable insight into separation of relevant energy scales in the problem. At the highest energy $\propto J_d$, the spin chains are real – spin fluctuations, as probed for example by the dynamic spin structure factor in inelastic neutron scattering experiments, have a strong one-dimensional character and mostly propagate along one of the three available chain directions. This interesting feature is, however, strongly masked by the hexagonal symmetry of the lattice: to the untrained eye excitations running at $\pm 120^\circ$ to each other will probably appear as almost isotropic two-dimensional modes. Even more importantly, at this high energy spin excitations are *fractionalized* – they are the spin-1/2 spinons of the emergent spin chains. This immediately implies that in inelastic neutron scattering experiments they show up as a broad multi-particle continuum extending up to energy $\propto \pi J_d$. Kinematic effects, of the kind described previously for structurally-anisotropic antiferromagnet Cs_2CuCl_4 [47], may produce coherent spin-1 triplon excitations in some parts of the Brillouin zone.

At much lower energy $\propto J_{1,2}$, the two-dimensional cuboc order sets in. One-dimensional spinons bind into spin-1 spin waves which propagate truly isotropically in the kagomé lattice. The energy-dependent evolution of spinons into spin waves is quite complex and represents a challenging open theoretical problem, beyond the scope of this work, and relevant to many systems. Interestingly, in the vicinity of the compensated line $J_1 \approx J_2$ the characteristic energy scale for the two-dimensional cross-over is yet smaller, $\propto J_{1,2}^2/J_d \ll J_{1,2}$. In this VBC regime all spin excitations are gapped.

This brief description makes it clear that dynamic response of the model Hamiltonian (1) is very complex. It is expected to show a number of one-dimensional features, such as a broad incoherent continuum and strong dispersion along the three crystallographic chain directions. This, we insist, does not imply a spin-liquid ground state. Our extensive analytical and DMRG calculations find no evidence in support of the previously suggested [36] gapless chiral spin liquid states for $J_1 \neq J_2$ as well as of the decoupled chain state in the neighborhood of $J_1 = J_2$ line.

Turning now to the real material kapellasite, we observe that in the regime of parameters relevant to it [33, 34, 38], the ground state, according to our phase diagram Fig. 2, is the magnetically ordered cuboc2 phase rather than a spin liquid state. The experimentally observed spin liquid behavior [31, 32, 38] can be interpreted in two different ways. The first consists in the assumption that observed ‘spin-liquid’ features are remnants of the emergent high-energy spinons described above. The alternative explanation points out the importance of disorder which, according to recent NMR experiments, reaches a very large level – up to $\sim 25\%$ of spins are missing from the kagomé planes [32].

Interestingly, the ‘one-dimensional’ framework proposed

here can be straightforwardly applied to the analysis of disorder effects as well. The effect of non-magnetic disorder on a spin-1/2 chain is well understood [48] and its experimental manifestations in neutron scattering experiments have recently been identified in Ref. 49. It therefore seems that extending our ‘one-dimensional’ perspective to the kapellasite model with disorder is within reach. We leave such studies to the future.

Finally, the fact that established phase diagram does not include the previously suggested spin-liquid phase demonstrates the limitations of the frequently used parton mean-field approach, even when improved by Gutzwiller projection. It also shows that the accepted minimal kapellasite model (1) is not general enough to provide a new path to

spin-liquid phases of magnetic matter.

Acknowledgments

We acknowledge discussions with S. Bieri and C. Lhuillier. This research is supported by the state of Florida (S.S.G.), National Science Foundation Grants DMR-1157490 (S.S.G. and K.Y.), PREM DMR-1205734 (W.Z.), DMR-1442366 (K.Y.), DMR-1507054 (O.A.S.), DMR-1408560 (D.N.S), and DMR-1506119 (L.B.). We also acknowledge partial support from NSF Grant DMR-1532249 for computational resource.

-
- [1] L. Balents, *Nature* (London) **464**, 199 (2010), URL <http://www.nature.com/nature/journal/v464/n7286/full/nature08917.html>.
 - [2] L. Savary and L. Balents, ArXiv e-prints (2016), 1601.03742, URL <http://arxiv.org/abs/1601.03742>.
 - [3] P. Mendels, F. Bert, M. A. de Vries, A. Olariu, A. Harrison, F. Duc, J. C. Trombe, J. S. Lord, A. Amato, and C. Baines, *Phys. Rev. Lett.* **98**, 077204 (2007), URL <http://link.aps.org/doi/10.1103/PhysRevLett.98.077204>.
 - [4] J. S. Helton, K. Matan, M. P. Shores, E. A. Nytko, B. M. Bartlett, Y. Yoshida, Y. Takano, A. Suslov, Y. Qiu, J.-H. Chung, et al., *Phys. Rev. Lett.* **98**, 107204 (2007), URL <http://link.aps.org/doi/10.1103/PhysRevLett.98.107204>.
 - [5] M. A. de Vries, J. R. Stewart, P. P. Deen, J. O. Piatek, G. J. Nilsen, H. M. Rønnow, and A. Harrison, *Phys. Rev. Lett.* **103**, 237201 (2009), URL <http://link.aps.org/doi/10.1103/PhysRevLett.103.237201>.
 - [6] T.-H. Han, J. S. Helton, S. Chu, D. G. Nocera, J. A. Rodriguez-Rivera, C. Broholm, and Y. S. Lee, *Nature* (London) **492**, 406 (2012), URL <http://www.nature.com/nature/journal/v492/n7429/full/nature11659.html>.
 - [7] M. Fu, T. Imai, T.-H. Han, and Y. S. Lee, *Science* **350**, 655 (2015), ISSN 0036-8075, <http://science.sciencemag.org/content/350/6261/655.full.pdf>, URL <http://science.sciencemag.org/content/350/6261/655>.
 - [8] T.-H. Han, M. R. Norman, J.-J. Wen, J. A. Rodriguez-Rivera, J. S. Helton, C. Broholm, and Y. S. Lee, ArXiv e-prints (2015), 1512.06807, URL <http://arxiv.org/abs/1512.06807>.
 - [9] H. C. Jiang, Z. Y. Weng, and D. N. Sheng, *Phys. Rev. Lett.* **101**, 117203 (2008), URL <http://link.aps.org/doi/10.1103/PhysRevLett.101.117203>.
 - [10] S. Yan, D. A. Huse, and S. R. White, *Science* **332**, 1173 (2011), URL <http://www.sciencemag.org/content/332/6034/1173.full>.
 - [11] S. Depenbrock, I. P. McCulloch, and U. Schollwöck, *Phys. Rev. Lett.* **109**, 067201 (2012), URL <http://link.aps.org/doi/10.1103/PhysRevLett.109.067201>.
 - [12] H.-C. Jiang, Z. Wang, and L. Balents, *Nature Physics* **8**, 902 (2012), URL <http://www.nature.com/nphys/journal/v8/n12/full/nphys2465.html>.
 - [13] Y. Ran, M. Hermele, P. A. Lee, and X.-G. Wen, *Phys. Rev. Lett.* **98**, 117205 (2007), URL <http://link.aps.org/doi/10.1103/PhysRevLett.98.117205>.
 - [14] Y. Iqbal, F. Becca, S. Sorella, and D. Poilblanc, *Phys. Rev. B* **87**, 060405 (2013), URL <http://link.aps.org/doi/10.1103/PhysRevB.87.060405>.
 - [15] Y. Iqbal, D. Poilblanc, and F. Becca, *Phys. Rev. B* **89**, 020407 (2014), URL <http://link.aps.org/doi/10.1103/PhysRevB.89.020407>.
 - [16] L. Messio, B. Bernu, and C. Lhuillier, *Phys. Rev. Lett.* **108**, 207204 (2012), URL <http://link.aps.org/doi/10.1103/PhysRevLett.108.207204>.
 - [17] S.-S. Gong, W. Zhu, and D. Sheng, *Scientific reports* **4**, 6317 (2014), URL <http://www.nature.com/srep/2014/140910/srep06317/full/srep06317.html>.
 - [18] Y.-C. He, D. N. Sheng, and Y. Chen, *Phys. Rev. Lett.* **112**, 137202 (2014), URL <http://link.aps.org/doi/10.1103/PhysRevLett.112.137202>.
 - [19] B. Bauer, L. Cincio, B. P. Keller, M. Dolfi, G. Vidal, S. Trebst, and A. W. W. Ludwig, *Nature Communications* **5**, 5137 (2014), URL <http://www.nature.com/ncomms/2014/141010/ncomms6137/abs/ncomms6137.html>.
 - [20] S.-S. Gong, W. Zhu, L. Balents, and D. N. Sheng, *Phys. Rev. B* **91**, 075112 (2015), URL <http://link.aps.org/doi/10.1103/PhysRevB.91.075112>.
 - [21] W.-J. Hu, W. Zhu, Y. Zhang, S. Gong, F. Becca, and D. N. Sheng, *Phys. Rev. B* **91**, 041124 (2015), URL <http://link.aps.org/doi/10.1103/PhysRevB.91.041124>.
 - [22] A. Wietek, A. Sterdyniak, and A. M. Läuchli, *Phys. Rev. B* **92**, 125122 (2015), URL <http://link.aps.org/doi/10.1103/PhysRevB.92.125122>.
 - [23] K. Yang, L. K. Warman, and S. M. Girvin, *Phys. Rev. Lett.* **70**, 2641 (1993), URL <http://link.aps.org/doi/10.1103/PhysRevLett.70.2641>.
 - [24] W. Zhu, S. S. Gong, and D. N. Sheng, *Phys. Rev. B* **92**, 014424 (2015), URL <http://link.aps.org/doi/10.1103/PhysRevB.92.014424>.
 - [25] Y.-C. He and Y. Chen, *Phys. Rev. Lett.* **114**, 037201 (2015), URL <http://link.aps.org/doi/10.1103/PhysRevLett.114.037201>.
 - [26] Y.-H. Wu and H.-H. Tu, ArXiv e-prints (2016), 1601.02594, URL <http://arxiv.org/abs/1601.02594>.
 - [27] M. P. Zaletel, Z. Zhu, Y.-M. Lu, A. Vishwanath, and S. R. White, ArXiv e-prints (2015), 1511.01510, URL <http://arxiv.org/abs/1511.01510>.
 - [28] L. Cincio and Y. Qi, ArXiv e-prints (2015), 1511.02226, URL <http://arxiv.org/abs/1511.02226>.

- [29] R. Colman, C. Ritter, and A. Wills, *Chemistry of Materials* **20**, 6897 (2008), URL <http://pubs.acs.org/doi/abs/10.1021/cm802060n>.
- [30] R. Colman, A. Sinclair, and A. Wills, *Chemistry of Materials* **22**, 5774 (2010), URL <http://pubs.acs.org/doi/abs/10.1021/cm101594c>.
- [31] B. Fåk, E. Kermarrec, L. Messio, B. Bernu, C. Lhuillier, F. Bert, P. Mendels, B. Koteswararao, F. Bouquet, J. Ollivier, et al., *Phys. Rev. Lett.* **109**, 037208 (2012), URL <http://link.aps.org/doi/10.1103/PhysRevLett.109.037208>.
- [32] E. Kermarrec, A. Zorko, F. Bert, R. H. Colman, B. Koteswararao, F. Bouquet, P. Bonville, A. Hillier, A. Amato, J. van Tol, et al., *Phys. Rev. B* **90**, 205103 (2014), URL <http://link.aps.org/doi/10.1103/PhysRevB.90.205103>.
- [33] O. Janson, J. Richter, and H. Rosner, *Phys. Rev. Lett.* **101**, 106403 (2008), URL <http://link.aps.org/doi/10.1103/PhysRevLett.101.106403>.
- [34] H. O. Jeschke, F. Salvat-Pujol, and R. Valentí, *Phys. Rev. B* **88**, 075106 (2013), URL <http://link.aps.org/doi/10.1103/PhysRevB.88.075106>.
- [35] L. Messio, C. Lhuillier, and G. Misguich, *Phys. Rev. B* **83**, 184401 (2011), URL <http://link.aps.org/doi/10.1103/PhysRevB.83.184401>.
- [36] S. Bieri, L. Messio, B. Bernu, and C. Lhuillier, *Phys. Rev. B* **92**, 060407 (2015), URL <http://link.aps.org/doi/10.1103/PhysRevB.92.060407>.
- [37] Y. Iqbal, H. O. Jeschke, J. Reuther, R. Valentí, I. I. Mazin, M. Greiter, and R. Thomale, *Phys. Rev. B* **92**, 220404 (2015), URL <http://link.aps.org/doi/10.1103/PhysRevB.92.220404>.
- [38] B. Bernu, C. Lhuillier, E. Kermarrec, F. Bert, P. Mendels, R. H. Colman, and A. S. Wills, *Phys. Rev. B* **87**, 155107 (2013), URL <http://link.aps.org/doi/10.1103/PhysRevB.87.155107>.
- [39] O. A. Starykh, A. Furusaki, and L. Balents, *Phys. Rev. B* **72**, 094416 (2005), URL <http://link.aps.org/doi/10.1103/PhysRevB.72.094416>.
- [40] H. J. Schulz, *Phys. Rev. Lett.* **77**, 2790 (1996), URL <http://link.aps.org/doi/10.1103/PhysRevLett.77.2790>.
- [41] T. Hikihara and O. A. Starykh, *Phys. Rev. B* **81**, 064432 (2010), URL <http://link.aps.org/doi/10.1103/PhysRevB.81.064432>.
- [42] S. R. White, *Phys. Rev. Lett.* **69**, 2863 (1992), URL <http://link.aps.org/doi/10.1103/PhysRevLett.69.2863>.
- [43] I. McCulloch and M. Gulácsi, *Europhysics Letters* **57**, 852 (2002), URL <http://iopscience.iop.org/0295-5075/57/6/852>.
- [44] S. R. White, *Phys. Rev. B* **48**, 10345 (1993), URL <http://link.aps.org/doi/10.1103/PhysRevB.48.10345>.
- [45] S.-W. Tsai and J. B. Marston, *Phys. Rev. B* **62**, 5546 (2000), URL <http://link.aps.org/doi/10.1103/PhysRevB.62.5546>.
- [46] L. Messio, C. Lhuillier, and G. Misguich, *Phys. Rev. B* **87**, 125127 (2013), URL <http://link.aps.org/doi/10.1103/PhysRevB.87.125127>.
- [47] M. Kohn, O. A. Starykh, and L. Balents, *Nature Physics* **3**, 790 (2007).
- [48] S. Eggert and I. Affleck, *Phys. Rev. B* **46**, 10866 (1992), URL <http://link.aps.org/doi/10.1103/PhysRevB.46.10866>.
- [49] G. Simutis, S. Gvasaliya, M. Månsson, A. L. Chernyshev, A. Mohan, S. Singh, C. Hess, A. T. Savici, A. I. Kolesnikov, A. Piovano, et al., *Phys. Rev. Lett.* **111**, 067204 (2013), URL <http://link.aps.org/doi/10.1103/PhysRevLett.111.067204>.

Appendix A: Symmetries and transformations

Here we discuss the symmetries of the kagomé lattice. A sufficient set of generators for the full space group consists of two elementary translations, a \mathcal{C}_6 rotation about the center of a hexagon, and a reflection \mathcal{P} through a line passing through a site and a hexagon center. We begin with the description of these operations in terms of the primitive vectors \mathbf{a}_i given in the main text. Under the translations, we have

$$\begin{aligned}\mathcal{T}_1: \quad \mathbf{x} &\rightarrow \mathbf{x} + \mathbf{a}_1, \\ \mathcal{T}_2: \quad \mathbf{x} &\rightarrow \mathbf{x} + \mathbf{a}_2.\end{aligned}\quad (\text{A1})$$

The rotation and reflection act according to

$$\begin{aligned}\mathcal{C}_6: \quad \mathbf{a}_1 &\rightarrow -\mathbf{a}_{q-1}, \\ \mathcal{P}: \quad \mathbf{a}_1 &\leftrightarrow \mathbf{a}_2, \quad \mathbf{a}_3 \rightarrow \mathbf{a}_3.\end{aligned}\quad (\text{A2})$$

From these definitions, we can work out the action of these operations in the chain basis, in which a site is represented in the form (q, x, y) . Using the definitions of the sites, $\mathbf{x} = (x + \frac{1}{2})\mathbf{a}_q + y\mathbf{a}_{q+1}$, and keeping in mind the relation $\sum_q \mathbf{a}_q = 0$, we obtain for the translations

$$\begin{aligned}\mathcal{T}_1: \quad &\begin{cases} (1, x, y) \rightarrow (1, x+1, y) \\ (2, x, y) \rightarrow (2, x-1, y-1) \\ (3, x, y) \rightarrow (3, x, y+1) \end{cases} \\ \mathcal{T}_2: \quad &\begin{cases} (1, x, y) \rightarrow (1, x, y+1) \\ (2, x, y) \rightarrow (2, x+1, y) \\ (3, x, y) \rightarrow (3, x-1, y-1) \end{cases}.\end{aligned}\quad (\text{A3})$$

Under the point group operations we obtain

$$\begin{aligned}\mathcal{C}_6: \quad &(q, x, y) \rightarrow (q-1, -x-1, -y), \\ \mathcal{P}: \quad &\begin{cases} (1, x, y) \rightarrow (2, x-y, -y) \\ (2, x, y) \rightarrow (1, x-y, -y) \\ (3, x, y) \rightarrow (3, x-y, -y) \end{cases}.\end{aligned}\quad (\text{A4})$$

Now with this in hand, we can evaluate the transformations of the dimerization operators, $\varepsilon_{q,y} = \sum_x (-1)^x \mathbf{S}_{q,y}(x) \cdot \mathbf{S}_{q,y}(x+1)$. We find

$$\begin{aligned}\mathcal{T}_1: \quad &\begin{cases} \varepsilon_{1,y} \rightarrow -\varepsilon_{1,y} \\ \varepsilon_{2,y} \rightarrow -\varepsilon_{2,y-1} \\ \varepsilon_{3,y} \rightarrow \varepsilon_{3,y+1} \end{cases} \\ \mathcal{T}_2: \quad &\begin{cases} \varepsilon_{1,y} \rightarrow \varepsilon_{1,y+1} \\ \varepsilon_{2,y} \rightarrow -\varepsilon_{2,y} \\ \varepsilon_{3,y} \rightarrow -\varepsilon_{3,y-1} \end{cases}.\end{aligned}\quad (\text{A5})$$

and

$$\begin{aligned}\mathcal{C}_6: \quad &\varepsilon_{q,y} \rightarrow \varepsilon_{q-1,-y} \\ \mathcal{P}: \quad &\begin{cases} \varepsilon_{1,y} \rightarrow (-1)^y \varepsilon_{2,-y} \\ \varepsilon_{2,y} \rightarrow (-1)^y \varepsilon_{1,-y} \\ \varepsilon_{3,y} \rightarrow (-1)^y \varepsilon_{3,-y} \end{cases}.\end{aligned}\quad (\text{A6})$$

Finally, we can use this to give the transformation properties for W_q and V_q . Under translations,

$$\begin{aligned}\mathcal{T}_1: \quad &\begin{pmatrix} W_1 \\ W_2 \\ W_3 \end{pmatrix} \rightarrow \begin{pmatrix} -W_1 \\ -W_2 \\ W_3 \end{pmatrix}, \quad \begin{pmatrix} V_1 \\ V_2 \\ V_3 \end{pmatrix} \rightarrow \begin{pmatrix} -V_1 \\ V_2 \\ -V_3 \end{pmatrix} \\ \mathcal{T}_2: \quad &\begin{pmatrix} W_1 \\ W_2 \\ W_3 \end{pmatrix} \rightarrow \begin{pmatrix} W_1 \\ -W_2 \\ -W_3 \end{pmatrix}, \quad \begin{pmatrix} V_1 \\ V_2 \\ V_3 \end{pmatrix} \rightarrow \begin{pmatrix} -V_1 \\ -V_2 \\ V_3 \end{pmatrix},\end{aligned}\quad (\text{A7})$$

and under the point operations,

$$\begin{aligned}\mathcal{C}_6: \quad &W_q \rightarrow W_{q-1}, \quad V_q \rightarrow V_{q-1}, \\ \mathcal{P}: \quad &\begin{cases} W_1 \rightarrow V_2, & V_1 \rightarrow W_2 \\ W_2 \rightarrow V_1, & V_2 \rightarrow W_1 \\ W_3 \rightarrow V_3, & V_3 \rightarrow W_3 \end{cases}.\end{aligned}\quad (\text{A8})$$